Electronic Supplementary Material (ESI) for Physical Chemistry Chemical Physics.
This journal is © the Owner Societies 2022

Supporting Information — The role of interlayer gases and surface asperities in shock-induced intermetallic formation in Ni/Al nanocomposites.

Richard N.L. Terrett[1] and Terry J. Frankcombe*[1]

[1] *School of Physical, Environmental and Mathematical Sciences, UNSW-ADFA, Canberra, ACT, Australia.*

16 December 2021

1 Spatial binning

To inspect the spatial distribution of intensive properties, the system was divided into rectilinear bins by taking slices perpendicular to the long axis of the system (typically x). Where temperature is calculated, it is done by subtracting the center-of-mass velocity v_{CoM} of each bin from the individual atomic velocities of atoms contained within that bin, to account for the acceleration of slabs preceding impact and wave propagation.

2 Layer thickness estimation

Where nanolaminate layer thicknesses are reported, the mean layer thickness $\bar{\Lambda}$ is estimated *via* Eq. 1:

$$\bar{\Lambda}_i = \frac{V_i}{l_y l_z n_i} \tag{1}$$

Where V_i is the minimal bounding volume of atom type i, l_y and l_z are the supercell dimensions perpendicular to the lamination axis, and n_i is the number of monolayers of atom type i in the supercell. Minimal bounding volume is computed by surface mesh construction ([1] and references therein) around each atom type in OVITO, using a probe radius of 400 pm and 8 iterations of surface refinement. This measure of layer thickness is appropriate for rectilinear layers which are approximately consistent with the basis vectors of the supercell.

*Corresponding author. Email: t.frankcombe@adfa.edu.au.

Pair	ϵ_{ij} (/kJ·mol^{-1})	σ_{ij} (/pm)	$r_{eq.}$ (/pm)
Ar–Ar	1.001	340	382
Ar–Al	2.074	301	338
Ar–Ni	8.642	284	319

Table SI1: Lennard-Jones parameters for Ar, Al, and Ni.

3 Details on Lennard-Jones hybrid model for Ar

These potentials are adapted from those presented by Cheng and Lee, [2] and Sha, *et al.*, [3] using the Fender–Halsey combining rules [4] (Eqs 3, 4). These potentials are illustrated in Figure SI1.

$$V_{LJ}(r) = \begin{cases} 4\epsilon\left[(\frac{\sigma}{r})^{12} - (\frac{\sigma}{r})^{6} - (\frac{\sigma}{r_c})^{12} + (\frac{\sigma}{r_c})^{6}\right] & r < r_c \\ 0 & r \geq r_c \end{cases} \tag{2}$$

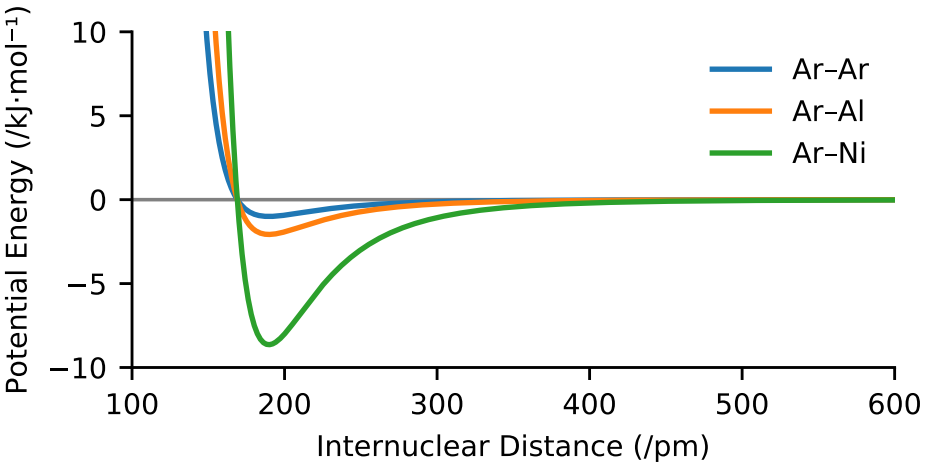

Figure SI1: Lennard-Jones pair potentials for Ar, Al, Ni as a function of internuclear separation. Potentials have been truncated and shifted such that $V_{LJ} = 0$ kJ·mol^{-1} at $r_c = 1$ nm (not shown).

$$\epsilon_{ij} = \frac{2\epsilon_i \epsilon_j}{\epsilon_i + \epsilon_j} \tag{3}$$

$$\sigma_{ij} = \frac{\sigma_i + \sigma_j}{2} \tag{4}$$

A typical equilibration containing an Ar fill according to the aforementioned model is given in Figure SI2.

The adsorption of Ar to Ni and Al slabs in RNLs was observed to generate Brunauer–Emmett-Teller (BET) multilayers at both metal surfaces. Illustrative histograms of Ar number density as a function of distance from metal surfaces and interlayer Ar number density are given in Figure SI3.

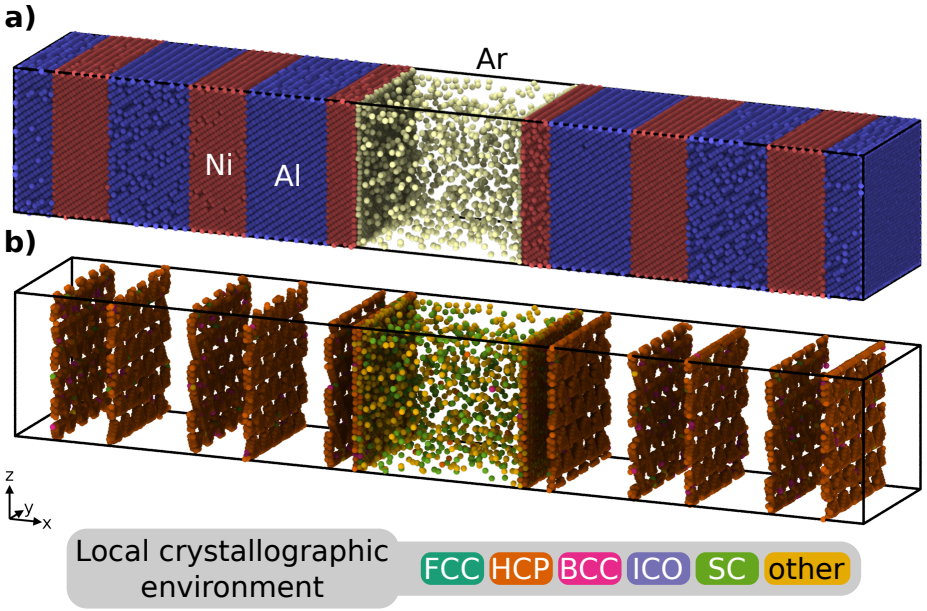

Figure SI2: **a)** Matched bilayers with nominal 10 MPa fill of Ar, after 1 ns equilibration with timestep of 10 fs under isothermal-isobaric ensemble (300 K, 0 Pa in y, z axes). Note the formation of Brunauer–Emmett-Teller (BET) adsorption layers of Ar. **b)** Crystallographic environment as determined by polyhedral template matching, with all atoms assigned as FCC removed.

		Number of atoms (/%)		
Surfaces	Ar atoms	N_{Al}	N_{Ni}	N_{Ar}
Al/Al	0	48.8	51.2	0.0
Al/Al	2000	48.5	50.9	0.6
Ni/Ni	0	48.5	51.5	0.0
Ni/Ni	2000	48.3	51.2	0.6
Ni/Al	0	48.5	51.5	0.0
Ni/Al	2000	48.3	51.2	0.6

Table SI2: Stoichiometry of flat surfaces with and without Ar fills.

3.1 Stoichiometry of flat impactors with and without interlayer argon

4 EDIP parameterisation for nitrogen interactions

Non-zero parameters for the N/Ni/Al EDIP potential described in the manuscript are given in Table SI3.

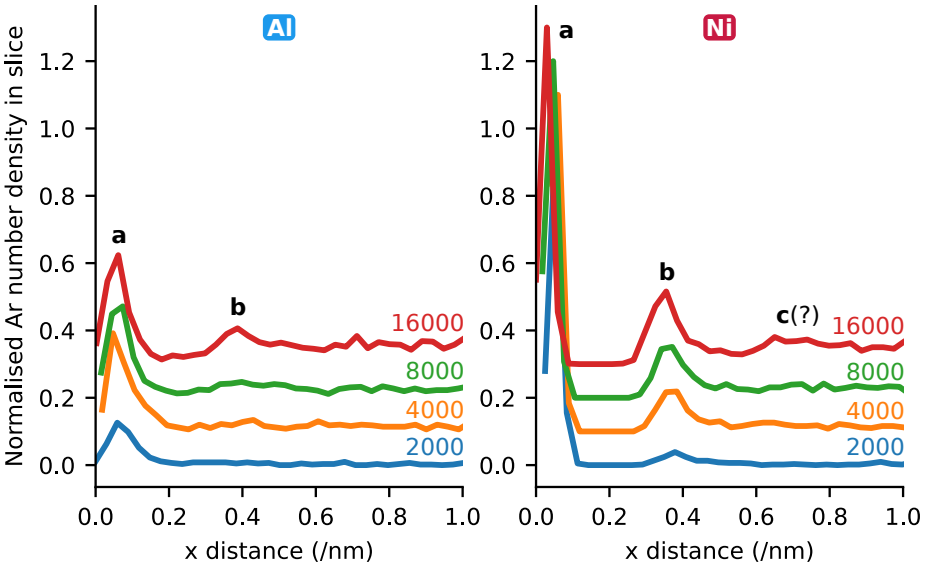

Figure SI3: Normalised number density of Ar near Ni and Al surfaces at different fills of Ar atoms. Successive data series have been shifted vertically by 10% for clarity. *n.b.* the higher affinity between Ni and Ar with respect to Al, as well as the BET adsorption multilayers (denoted **a**, **b**, and tentatively **c**) evident at both interfaces.

4.1 Details on generation and fitting of parameters for N/Ni/Al EDIP potential

EDIP potential parameters were generated using the Vienna *Ab initio* Simulation Package (VASP). Relevant citations are provided in the attached manuscript.

VASP calculations consisted of a suite of relaxed and unrelaxed total energy calculations on a range of periodic structures divisible into four main categories: **a)** bulk metal lattices with and without N inclusions, **b)** metal slabs with and without N inclusions, **c)** monatomic N and **d)** polyatomic N. In calculations where geometric optimisation was performed, optimisation included relaxation of ionic positions and unit cell basis vectors, using a conjugate gradients approach. Calculations employed randomised wavefunction initialisation, a plane wave energy cutoff of 3×10^2 eV, a total energy error convergence criterion of 5.0×10^{-6} eV, and Gaussian smearing of occupancies with $\sigma = 5.0 \times 10^{-2}$ eV. Wavefunction projection operators were evaluated in real space. Standard projector-augmented wave (PAW) pseudopotentials as supplied by the VASP package (`PAW Ni_GW 31Mar2010`, `PAW Al_GW 19Mar2012`, `PAW_PBE N 08Apr2002`) were used. These pseudopotentials employ the Perdew–Burke–Ernzerhof combined GGA exchange–correlation density functional.

K-points were automatically generated according to the Monkhorst–Pack scheme, [5] centered on the origin Γ of the Brillouin zone. A varying number of K-points was employed for each calculation type: $2 \times 2 \times 2$ for monatomic N and metallic bulks, $2 \times 2 \times 1$ for metallic slabs, and $1 \times 1 \times 1$ for polyatomic N in the x, y, and z directions respectively.

Complementary calculations of lattice energy were undertaken in LAMMPS using the 2009 EAM potentials of Purja Pun and Mishin.[6] Potential fitting was achieved through a program wrapping a general-purpose simulated annealing subroutine published by William 'Bill' Goffe. [7]

82 geometries were employed to obtain the fitting. These geometries are divided into several sets:

1. Bulk Ni, Al, and B2 NiAl lattices.
2. Ni, Al, and B2 NiAl lattices with mononuclear nitrogen inclusions.
3. Ni and Al slabs with mono- and dinuclear nitrogen inclusions.
4. Isolated N and N_2 assemblages.

An explanatory subset of these configurations is illustrated in Figure SI4. Geometries and corresponding VASP energies for each configuration are provided in the file `fit-geoms.tar.gz`.

5 Time series and spatial histograms of RNL collisions with interlayer N_2

Time series of Ni/Al RNL collisions with an interlayer nitrogen fill are illustrated in Figure SI6.

	Interaction			
Parameter	**N–Ni–Ni**	**N–Al–Al**	**N–N–N**	Units
A	3.645284×10^{1}	1.408193×10^{1}	7.899020×10^{1}	eV
B	6.791469×10^{-1}	1.186439	8.303978×10^{-1}	Å
r_a	3.001274	3.453207	3.178649	Å
r_c	2.407509	1.701310	7.817105×10^{-1}	Å
α	1.499806×10^{2}	4.312808	4.381870	
β	2.548526×10^{-3}	3.085868×10^{-2}	1.601516×10^{-1}	
η	7.100192×10^{-1}	1.242801×10^{1}	1.877102×10^{1}	
γ	1.524090	3.745907	2.053574	
λ	4.225363	3.296537×10^{1}	2.812451	Å
μ	9.924282×10^{-1}	8.926755×10^{-1}	4.728853	eV
τ	1.594402×10^{-1}	9.999864	8.949286	
σ	5.501664×10^{-1}	1.889386	4.185799	Å
Q_0	3.336155×10^{3}	1.407911×10^{2}	4.072389×10^{3}	
u_1	−1.327979	-1.404322×10^{-2}	−2.370404	
u_2	2.963824×10^{1}	3.480841×10^{2}	2.391353×10^{1}	
u_3	4.598414×10^{-1}	5.782318×10^{-2}	6.465032×10^{-1}	
u_4	3.445069×10^{1}	1.309372	3.588246×10^{-1}	

Table SI3: Numerical values for EDIP parameterisation of N–Ni–Ni, N–Al–Al, and N–N–N three-body interactions.

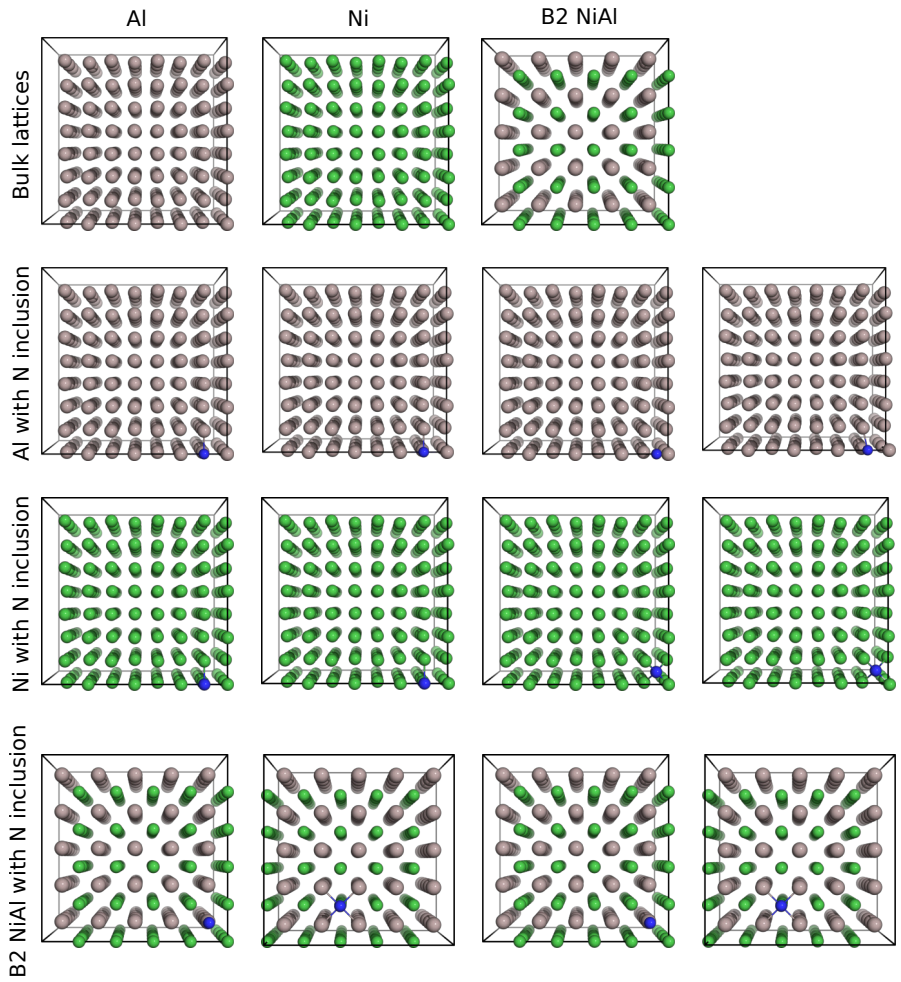

Figure SI4: Exemplary subset of bulk Ni, Al, and B2 NiAl lattices with and without nitrogen inclusions, used as fitting data for EDIP parameterisation.

References

[1] A. Stukowski. "Computational Analysis Methods in Atomistic Modeling of Crystals". In: *JOM* 66.3 (Dec. 2013), pp. 399–407. DOI: 10.1007/s11837-013-0827-5.

[2] Y.Y. Cheng and C.C. Lee. "Molecular dynamics simulations of argon cluster impacts on a nickel film surface". In: *Nuclear Instruments and Methods in Physics Research Section B: Beam Interactions with Materials and Atoms* 267.8-9 (May 2009), pp. 1428–1431. DOI: 10.1016/j.nimb.2009.01.056.

[3] H. Sha et al. "Molecular simulation study of aluminum-noble gas interfacial thermal accommodation coefficients". In: *AIChE Journal* 64.1 (Aug. 2017), pp. 338–345. DOI: 10.1002/aic.15886.

[4] B.E.F. Fender and G.D. Halsey. "Second Virial Coefficients of Argon, Krypton, and Argon-Krypton Mixtures at Low Temperatures". In: *The Journal of Chemical Physics* 36.7 (Apr. 1962), pp. 1881–1888. DOI: 10.1063/1.1701284.

[5] H.J. Monkhorst and J.D. Pack. "Special points for Brillouin-zone integrations". In: *Physical Review B* 13.12 (June 1976), pp. 5188–5192. DOI: 10.1103/physrevb.13.5188.

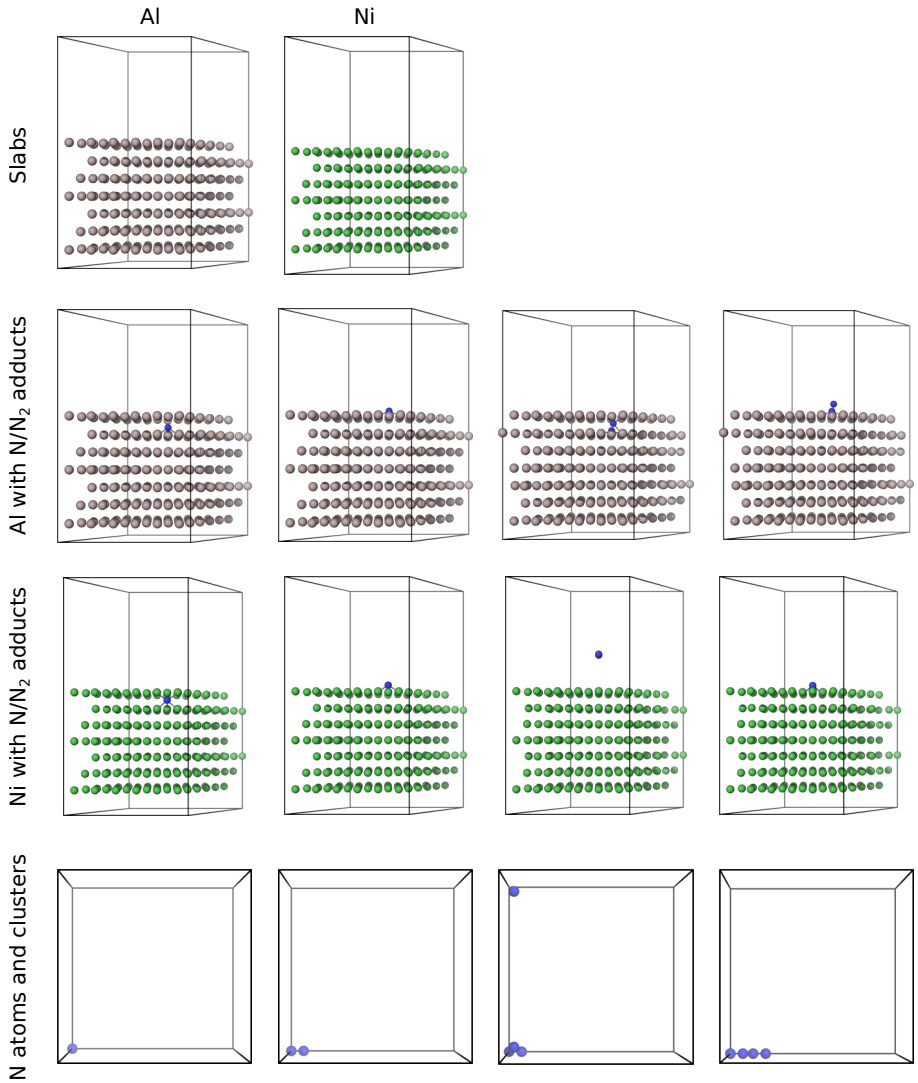

Figure SI5: Exemplary subset of Ni and Al slabs with and without surfacial and interstitial nitrogen, used as fitting data for EDIP parameterisation.

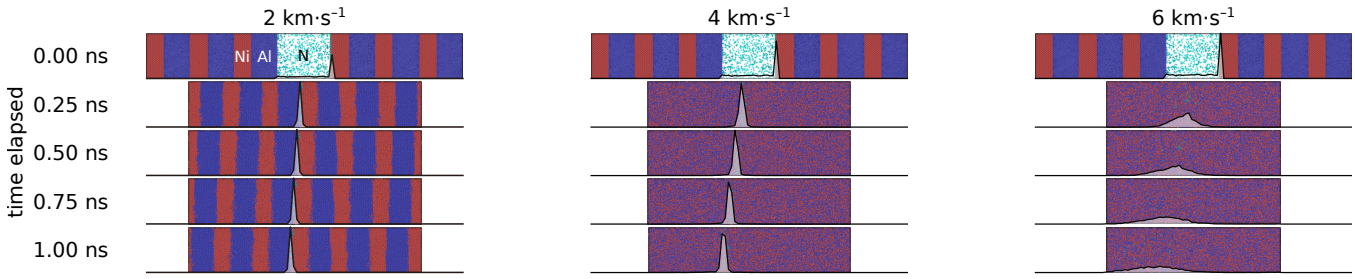

Figure SI6: Time series of Ni/Al laminate collisions at 2–6 km·s^{-1}. Normalised nitrogen number density as a function of position is indicated by overlaid histograms. *n.b.* the initial interlayer nitrogen distribution is asymmetric, as reflected by the histogram. All calculations were undertaken with an integrator timestep of 0.25 fs.

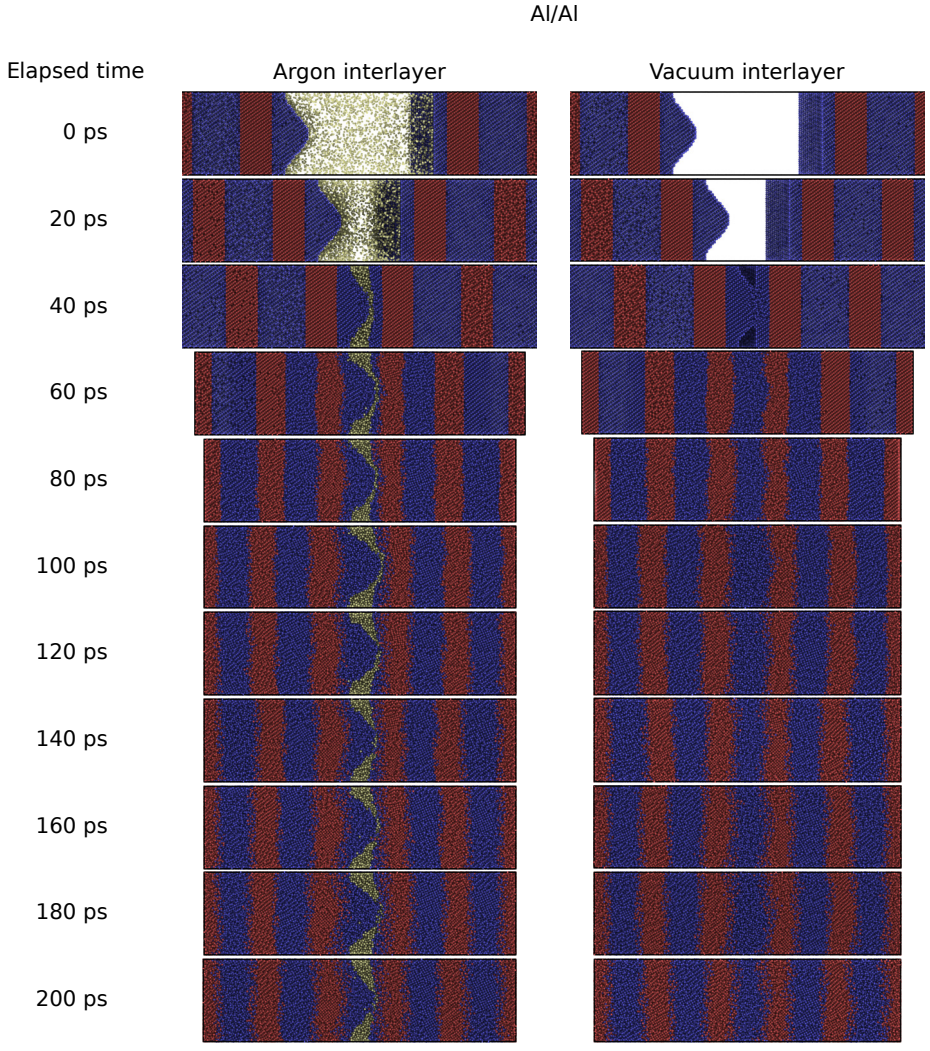

Figure SI7: Time evolution of impact of perpendicular Al/Al asperities with and without Ar interlayer, at a relative collision velocity of 2 km · s^{-1}.

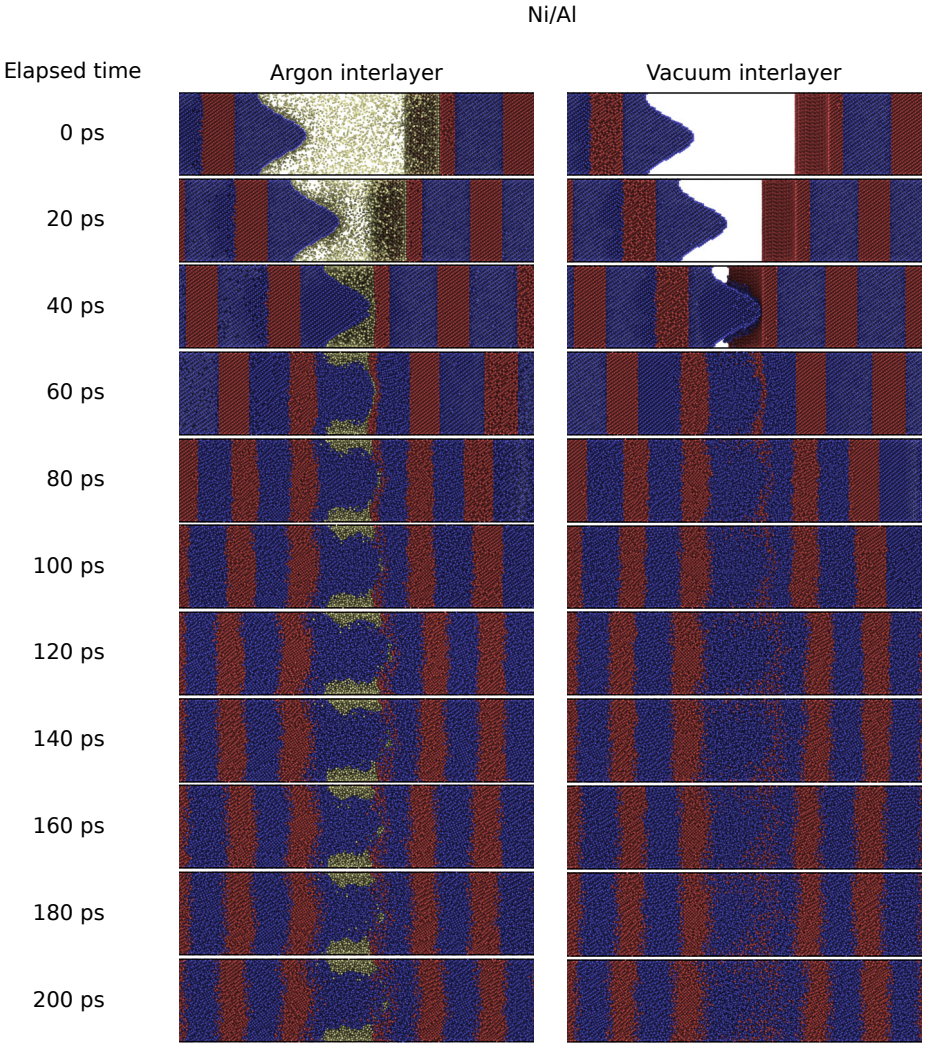

Figure SI8: Time evolution of impact of perpendicular Ni/Al asperities with and without Ar interlayer, at a relative collision velocity of $2\,\mathrm{km}\cdot\mathrm{s}^{-1}$.

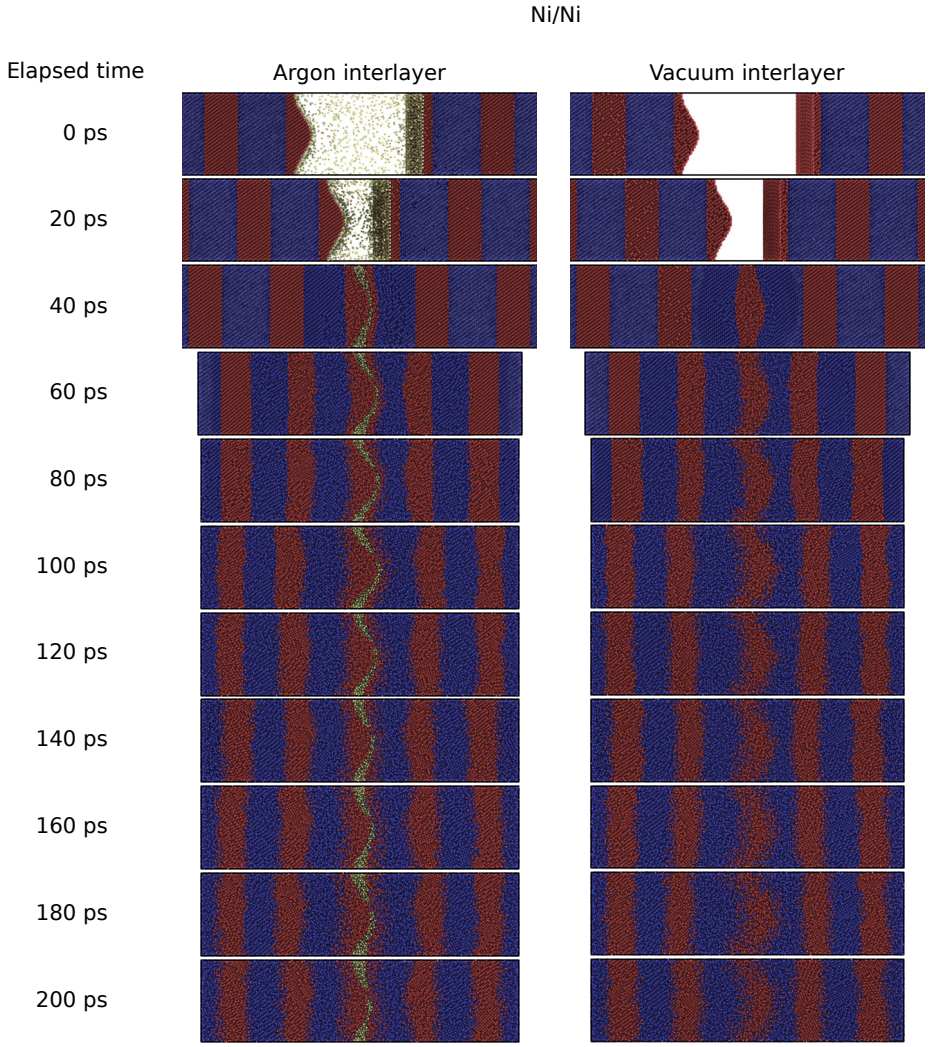

Figure SI9: Time evolution of impact of perpendicular Ni/Ni asperities with and without Ar interlayer, at a relative collision velocity of $2\,\mathrm{km}\cdot\mathrm{s}^{-1}$.

[6] G.P. Purja Pun and Y. Mishin. "Development of an interatomic potential for the Ni-Al system". In: *Philosophical Magazine* 89.34-36 (Dec. 2009), pp. 3245–3267. DOI: 10.1080/14786430903258184.

[7] W.L. Goffe, G.D. Ferrier and J. Rogers. "Global optimization of statistical functions with simulated annealing". In: *Journal of Econometrics* 60.1-2 (Jan. 1994), pp. 65–99. DOI: 10.1016/0304-4076(94)90038-8.